Phys. Status Solidi A **212,** No. 7, 1607–1614 (2015) / **DOI** 10.1002/pssa.201532305

physica status solidi a
www.pss-a.com
applications and materials science

Hot-wire assisted ALD of tungsten films: *In-situ* study of the interplay between CVD, etching, and ALD modes

Mengdi Yang*, Antonius A. I. Aarnink, Alexey Y. Kovalgin, Rob A. M. Wolters, and Jurriaan Schmitz

MESA+ and Institute for Nanotechnology, University of Twente, P.O. Box 217, 7500AE Enschede, The Netherlands

Received 2 March 2015, revised 30 April 2015, accepted 30 April 2015
Published online 25 May 2015

Keywords atomic layer deposition, etching, hot wire, *in-situ* spectroscopic ellipsometer, thin films, tungsten

* Corresponding author: e-mail m.yang@utwente.nl, Phone: +31 534 895 215

In this work, we investigated an approach of hot-wire assisted ALD (HWALD), utilizing a hot (up to 2000 °C) tungsten (W) wire. Tungsten films were deposited by this method using alternating pulses of WF_6 gas and atomic hydrogen (at-H). The latter was generated by catalytic dissociation of molecular hydrogen (H_2) upon the hot-wire. The W films were grown on a 100-nm thick thermal SiO_2. The growth process was monitored in real time by an *in-situ* spectroscopic ellipsometer (SE). The real-time SE monitoring revealed the coexistence of three processes: CVD, etching, and ALD of the W film. WF_6 could back-stream diffuse to the hot-wire, resulting in WF_6 decomposition and generation of a flux of fluorine (F). The latter caused etching of the grown W film and the filament, and provided extra tungsten supply, which might cause CVD. Higher pressure and higher carrier gas flow rate were found to largely suppress the back-stream diffusion of WF_6, which efficiently limited CVD. By controlling the dose of WF_6 and process pressure, the etching had also been minimized. X-ray photoelectron spectroscopy of optimized HWALD grown W revealed 99 at% of W; concentrations of oxygen and fluorine were lower than 1%, below the detection limit.

1 Introduction Manufacturing of semiconductor devices, such as microprocessors, DRAM memories, flash memories, and image sensors, relies on deposition of thin dielectric, semiconductor, and metallic layers (films) of various functionalities. Atomic layer deposition (ALD) is becoming a major player in the field of deposition. The most important advantage of ALD over other deposition techniques is its capability of depositing films of uniform thickness on arbitrarily shaped and patterned surfaces, and controlling the thickness with a very high precision [1]. The combination of these two features is demanded for e.g., future 3D integration. A reduced processing temperature, natural to ALD, additionally allows the manufacturing of devices by post-processing of electronic chips.

Single-element films of metals and semiconductors, crucially important for the industry, are however very difficult to deposit using thermal-only ALD processes [1]. A solution in this case is Plasma-enhanced ALD (PEALD), also called radical-enhanced ALD (REALD). Hydrogen- or nitrogen-based plasmas are used to deposit Ta(N), Ti(N), Ru, Si, and Ge [1], Al [2] as well as AlN [3] and GaN [4]. Pt can be grown using remote O_2 plasmas [5]. However three limitations make PEALD less attractive. The first is a reduced step coverage compared to thermal ALD, caused by radical recombination away from the plasma. The second limitation is that plasmas cause damage to the wafer under treatment, in particular to MOS transistors. A common solution, i.e., employing a remote plasma, is in this case difficult to apply due to increased reactor volumes leading to long ALD cycle times. Additionally, radical recombination can occur during their delivery from the plasma to the wafer surface. Finally, even simple one- or two-gas plasmas can cause numerous chemical reactions. As a result, the wafer surface is exposed to various ions, radicals, and atoms, as well as UV photons [6]. This makes the composition and structure of the growing film hard to predict and control. When the chemistry of the surface reactions is influenced by both plasma and gas dynamics, the process control complexity increases even further.

In this work, we propose an alternative method to generate radicals by means of a hot-wire (hot filament). It is well known that dissociation of a certain gas precursor to

form radicals can be achieved due to reactions on a hot tungsten (W) filament [7, 8]. For example, W filament heated up to 1500–2000 °C has been reported as an effective tool to decompose molecular hydrogen (H_2) [9–11] and NH_3 [12]. By using a hot-wire instead of a plasma, we aim to achieve a better control ("monochromatization") of the reactant supply in a hot-wire ALD (HWALD) reactor. As a matter of fact, publications related to HWALD are very rare in the literature. The few available works are on HWALD of Co(W) films [13, 14], where ammonia gas is dissociated upon hot-wire. Kostis et al. [15] introduced oxygen gas to oxidize hot tungsten filament and form volatile tungsten oxides. The oxides were further transported to the substrate, resulting in WO_x deposition. In our approach, we attempt to grow metallic tungsten (W) by sequential exposures to WF_6 and atomic hydrogen, utilizing self-limiting surface reactions. To emphasize, the hot-wire itself is not aimed to be a source of tungsten precursors in our case; it only provides atomic hydrogen.

Tungsten has been found to be attractive for making vias in ultra large scale integration (ULSI) technology due to its inertness to many chemicals, compatibility with silicon technology and the low electrical resistivity [16]. In this paper, we discuss on the deposition of tungsten films by HWALD using sequential pulses of WF_6 gas and atomic hydrogen (at-H). The latter is generated by dissociation of H_2 on the hot-wire.

2 Experimental

2.1 HWALD reactor A schematic cross-section of the home-built HWALD reactor is shown in Fig. 1. Molecular hydrogen (H_2) carried by argon gas (Ar) was introduced into the chamber via the hot-wire port (top). WF_6 carried by Ar was admitted via the gas ring a few cm above the substrate. For the hot-wire a pure W filament was used, which could be heated resistively. The reactor was equipped with a spectroscopic ellipsometer (SE), Woollam M-2000 of J. A. Woollam Co., Inc., combined with CompleteEASE software. The SE enabled *in-situ* monitoring of the deposition process in real time. It appears from both experiments and simulations that a W film thinner than 30 nm is sufficiently transparent for SE measurements.The distance between the at-H outlet and the substrate was approximately 70 cm. To note, the efficient delivery of at-H from the hot-wire to substrate in the pressure range studied in this work was previously confirmed by separate experiments on etching of tellurium (Te) films by at-H [17]. The advantage of this design, despite a long diffusion distance required, was that the wafer could be protected from the damage caused by the hot-wire radiation.

The HWALD chamber (reactor 1) could be evacuated to a base pressure of 10^{-7} mbar by a turbomolecular pump. Maximum temperature of the substrate holder was 400 °C. High-speed ALD valves were used, with a time resolution of 0.1 s. Importantly, deposition of a seed layer (W), necessary for the subsequent HWALD of W, was carried out in a separate reactor (reactor 2, see Ref. [17] for reactor details). The two reactors, utilized in this work, were connected to each other via a loadlock with a base pressure of 10^{-7} mbar. This enabled the wafer transfer without vacuum break, ensuring no interface deterioration

2.2 Hot-wire temperature calibration In our experiment, hot-wire (i.e., a tungsten filament) temperature was established by applying a voltage across it, while current was fixed at maximum, to ensure a variable power dissipation. The irradiative hot-wire temperature was measured by a pyrometer. Figure 2 shows a calibration curve for the temperature as a function of applied power. The experiments were conducted in the power range of 138–336 W, corresponding to the temperature range of 1500–2000 °C.

It is noteworthy that the hot-wire exhibited a good stability and reproducibility of the calibration curve after hundreds of hours operation. Moreover, it is known from the literature that the dissociation probability of H_2 rises with

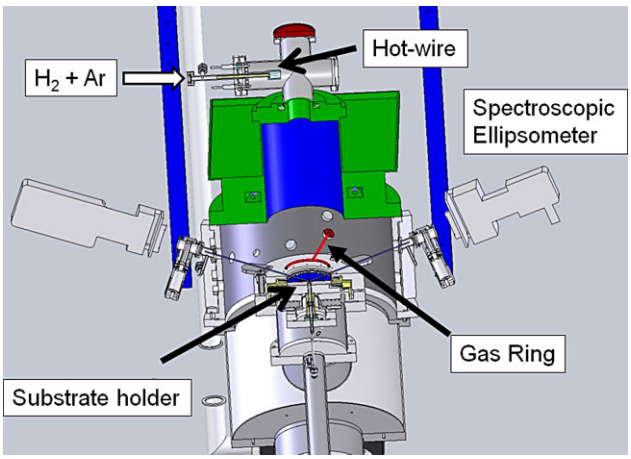

Figure 1 A schematic cross-sectional view of the cold-wall HWALD reactor (reactor 1) used in this study. The spectroscopic ellipsometer is installed at a fixed angle of 73°.

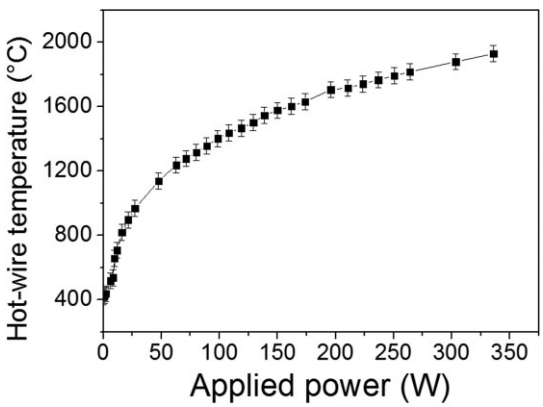

Figure 2 A curve presenting the relationship between hot-wire temperature (measured by a pyrometer) and applied power.

the increasing hot-wire temperature, and can reach a maximum at around 2700 °C [18].

2.3 Sample preparation In this experiment, tungsten films were deposited on a 100-nm-thick silicon oxide (SiO_2) thermally grown on p-type Si (100) substrate. Standard substrate cleaning included 10 min dipping in a 99% HNO_3 (room temperature), rinsing, and 10 min dipping in a 69% HNO_3 (95 °C). Finally, the substrate was immersed into a 0.3% HF solution for 3 min. As the adhesion is very poor between tungsten and SiO_2 or Si_3N_4 [19], an adhesion layer is required [20]. In this work, a thin (<10 nm) layer of amorphous silicon (a-Si) was first deposited on SiO_2 by chemical vapour deposition (CVD) using disilane (Si_2H_6), at 325 °C and a pressure of 10 mbar. The thickness of a-Si was *in-situ* monitored by SE. Next, the reactor was pumped down to a pressure of 1 mbar followed by introducing WF_6 to convert the a-Si into W. Further, the reactor was flushed by N_2 for 10 min and evacuated back to 10^{-7} mbar, followed by the wafer transfer to the HWALD reactor 1, to continue with the ALD process. The HWALD of W films was carried out using sequential pulses of WF_6 and at-H at substrate temperatures ranging between 200 and 325 °C, and process pressures of 0.001–1 mbar. For *ex-situ* (electrical) characterization, it is important to prevent oxidation of the grown W film during its exposure to air. The wafer was therefore transferred back to reactor 2, where a 5–10 nm capping layer of a-Si was deposited (same deposition method as used for a-Si seed layer) on top of W, completing the process.

2.4 Thickness measurement Thickness of the layers was monitored by *in-situ* spectroscopic ellipsometer in real-time. The SE covered the spectral range from 245 to 1688 nm with a resolution of 1.6 nm. The measurement data were acquired throughout the growth process every 5 s. The optical SE model, used to extract thickness and optical constants of W layers, is shown in Table 1. In this model, the required optical constants of the Si substrate, SiO_2 and a-Si were provided by the software database; the thicknesses were fitted by SE. The surface roughness was obtained by Bruggeman effective medium approximation (EMA), comprising 50% of voids and 50% of the corresponding material. The W seed layers were modelled by introducing six Lorentz oscillators [24], whereas the HWLAD W layers required only two Lorentz oscillators and one Drude term [25, 26].

Table 1 Layer stack, included in the optical SE model to extract thickness of the grown W.

layer	material	fitting parameters
roughness	Bruggeman EMA	thickness
capping layer	a-Si [21]	thickness
ALD W layer	oscillators	optical constants and thickness
W seed layer	oscillators	optical constants and thickness
SiO_2 layer	SiO_2 [22]	thickness
Si substrate	Si substrate [23]	temperature

To increase the accuracy of *in-situ* SE measurements, first the SiO_2/Si substrate was *in-situ* measured by SE after its loading; the corresponding model parameters have been fixed. Every next deposited layer (a-Si, W, a-Si) has been subsequently added to the existing model, measured by SE and then again fixed in the model. This minimized the uncertainty of determining thicknesses of several sub-layers included in the stack. For selected samples the thickness measured by SE was verified by helium ion microscope (HIM), or by X-ray reflection (XRR). In Fig. 3 an HIM image of a W layer on SiO_2 is shown. A thickness of 20 nm is indicated, whereas the SE measurements also revealed a thickness of 20 nm, with a roughness of 3.2 nm. Thickness obtained by XRR also showed a good agreement with an error of about 10%. This supported the validity of the SE model.

3 Results and discussion

3.1 The existence of CVD and etching modes From the literature, thermal dissociation of WF_6 (in gas phase) starts at 750 °C [27, 28]. Although the gas ring was installed at a distance of 70 cm below the hot-wire, the operating conditions (pressure, gas flows) could greatly influence the upward diffusion of WF_6 to the hot-wire. As a consequence, this WF_6 will dissociate at the hot-wire, likely generating, among others, atomic fluorine (at-F). As the dissociation of WF_6 occurs in equilibrium, any increase of concentration of WF_6 will enhance the generation of at-F. It is reported that the lifetime of at-F can be quite long [29]. Additionally, both WF_6 and fluorine can adsorb on the (cold) reactor walls. This provides a background supply of WF_6 and fluorine to the gas phase over the deposition cycles. Fluorine, generated from WF_6 dissociation upon the hot-wire, can contribute to etching the hot-wire and regeneration of volatile tungsten precursor(s) (likely tungsten fluorides). When mixed with at-H, these precursors may contribute to a CVD mode at substrate level. The

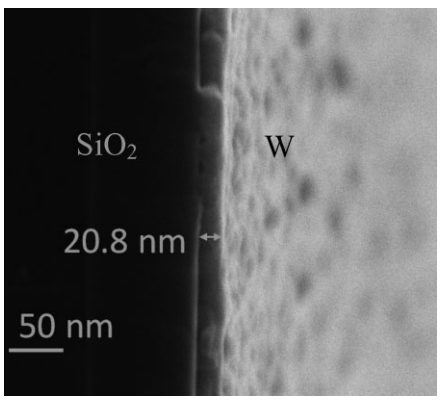

Figure 3 Helium ion microscopy image (cross-section) of a W film on SiO_2/Si. To compare, the W thickness given by SE is 20 nm, with an estimated roughness of 3.2 nm.

experiments shown in Fig. 4 confirm the existence of a CVD mode. For example a 1-min exposure to WF_6 gas followed by a 2-min purge and subsequent to at-H reveals a continuous growth of W film up to 2.5 nm in thickness (filament temperature of 1910 °C). This occurs during the entire (up to 25 min) exposure to at-H only, likely due to CVD.

Figure 4(a–d) shows the CVD growth under different conditions, while substrate temperature and total pressure were fixed at 325 °C and 0.01 mbar. Firstly, in Fig. 4(a) the growth rate increases with hot-wire temperature due to the improved dissociation efficiency of H_2 [18], resulting in a higher at-H flux. However, the difference between 1860 and 1910 °C is small, probably due to the limited reactant (i.e., volatile tungsten precursors) supply. From Fig. 4(b), there is no significant impact of the H_2 gas flow rate, likely pointing to a comparable amount of at-H reaching the substrate surface in these cases. However, our experiments (not shown) indicate that the upstream diffusion of WF_6 can be suppressed by a higher hot-wire gas flow from top to the reactor bottom. So, to minimize CVD, the flow rate of H_2 is determined to be 100 sccm (maximum in our case). From Fig. 4(c), a higher flow of the initial WF_6 enhances the growth rate. It is noticeable that the growth rate in the first 5 min doubles when the WF_6 flow rate becomes two times larger, implying that the initial 0–10 min growth is mainly influenced by the WF_6 injected from the gas ring. On the contrary, growth rates for times exceeding approximately 20 min are almost the same despite the different WF_6 flow rates. Analyzing the curves (values and shapes), one can conclude that the growth rates after an exposure of around 20 min follow the kinetics of desorption of the reactants that adsorbed on the cold walls during the preceding WF_6 pulse(s). In Fig. 4(d), it is shown that the flow rate of H_2-carrier gas has a significant effect. Apparently, a higher downward flow rate could (i) suppress the upward diffusion of the reactants, thereby decreasing their interaction with the hot wire, (ii) decrease the partial pressures of reactants and thus suppress the related CVD mode, and (iii) shorten the delivery time of at-H to the substrate. As a matter of fact, a 10-times higher Ar flow decreases the growth rate in approximately two to four times, depending on the time of exposure to at-H. The elemental composition of the as-grown film, obtained by X-ray photoelectron spectroscopy (XPS), is presented in Fig. 5. One should note the remarkably low (i.e., at detection limits) concentrations of all impurities and the concentration of tungsten at 92–98 at%. It is quite clear that the continuous deposition of W films up to 2.5 nm manifests a permanent source of tungsten in gas phase, most probably in the form of WF_6. As mentioned above, this source is expected due to outgassing of reactants from the reactor cold walls.

The impact of total gas pressure on the growth rate was additionally studied, see Fig. 6. On one hand, a higher pressure is expected to increase the recombination of at-H [30] and to suppress the upward diffusion. On the other hand, a higher (partial) pressure of WF_6 will shift the

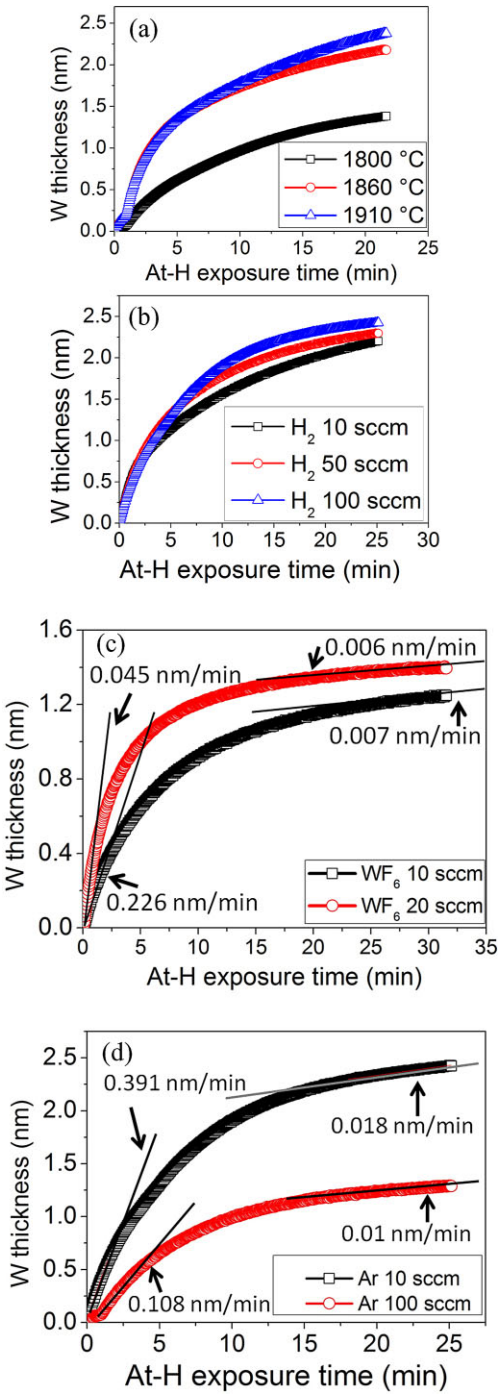

Figure 4 Film growth (obtained by *in-situ* SE) versus different deposition parameters. All long-time exposures to at-H were performed after a 1-min exposure to WF_6 gas followed by a 2-min purge. Standard parameter values: 0.01 mbar of pressure, 325 °C of substrate temperature, 1860 °C of hot-wire temperature, 100 sccm of H_2, 10 sccm of WF_6, 100 sccm of H_2-carrier gas (Ar), and 50 sccm WF_6-carrier gas (Ar). Each graph shows the influence of one parameter only while keeping the standard values for all other parameters. The figure shows the influence of: (a) hot-wire temperature, (b) H_2 flow rate, (c) WF_6 flow rate, and (d) H_2-carrier-gas (Ar) flow rate.

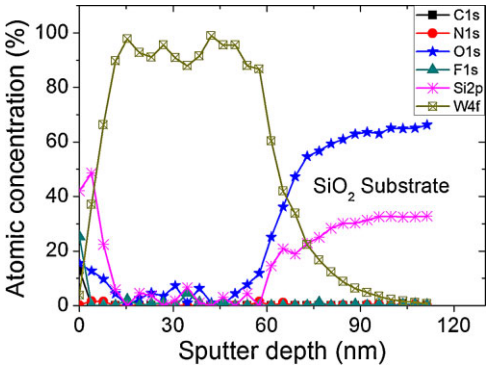

Figure 5 XPS-profile of the film grown at 0.01 mbar with the following cycle sequence: 2.5 min WF_6/2 min purge/10 min at-H/ 2 min purge. Flow rates of WF_6 and H_2 were 5 and 100 sccm, respectively. Other conditions: hot-wire temperature of 1800 °C, substrate temperature of 325 °C, Ar-carrier-gas flows for WF_6 and H_2 of 50 and 100 sccm, respectively. The Si signal at the beginning is from the a-Si capping layer.

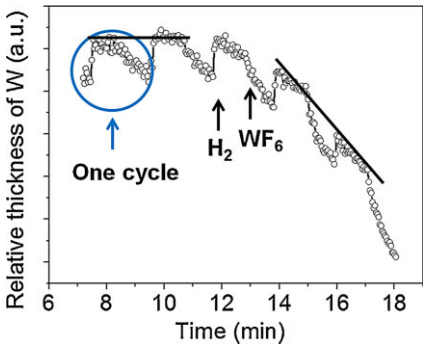

Figure 7 *In-situ* monitoring of individual pulses by SE. Black lines indicate the slopes. The arrows show the admittance of the corresponding gas pulses to the reactor. One cycle consisted of 0.1 s at-H exposure, 60 s of purge, 0.1 s of WF_6 exposure, and 60 s purge. Conditions: 1 mbar of pressure, 325 °C of substrate temperature, 1750 °C of hot-wire temperature, 100 sccm Ar carrier gas of H_2, 50 sccm Ar carrier gas of WF_6, and 100 sccm of H_2 and 10 sccm of WF_6. Due to the short pulse times of at-H and WF_6, the last two flow rates cannot be accurately measured.

equilibrium towards generating more fluorine. Consequently, a suppression of the CVD mode and the growth can be expected. This is confirmed in Fig. 6 that a pressure of 0.3 mbar sufficiently decreases the CVD growth.

To conclude, the H_2 and top-carrier-gas flow rates were chosen both at 100 sccm (maximum values), in combination with high enough process pressure, to minimize the possible CVD mode. Moreover, the WF_6 dose should be kept short, to limit the unwanted supply of reactants enhancing CVD. This can be achieved by limit WF_6 pulse time and flow rate.

3.2 Etching mode of deposited W films Fluorine, generated by the decomposition of WF_6 on the hot-wire, will diffuse downwards and etch the deposited W film. This effect was more pronounced at high WF_6 pressures, due to the mentioned shift of equilibrium. The interplay between growth and etching modes is presented in Fig. 7. The high sensitivity of in-situ SE allows study of the separate ALD cycles (0.1 s at-H, 60 s purge, 0.1 s WF_6, and 60 s purge). Pulses of at-H and WF_6 are indicated. One can clearly see a gradually increasing decay of the thickness after introducing every next WF_6 pulse, i.e., etching. In the first two cycles starting from 0.23 nm at 7 minutes, the growth rate (H_2 pulse) is approximately equal to the etching rate (WF_6 pulse), resulting in near-zero net growth of the film. From the third cycle, etching starts to increasingly dominate, leading to the net decline of the film thickness. This behaviour, typical and reproducible for given conditions, can be explained by a gradual increase of fluorine concentration in the reactor due to the preceding WF_6 pulses. This highlights the importance of limiting the WF_6 dose during each pulse, in order to minimize etching.

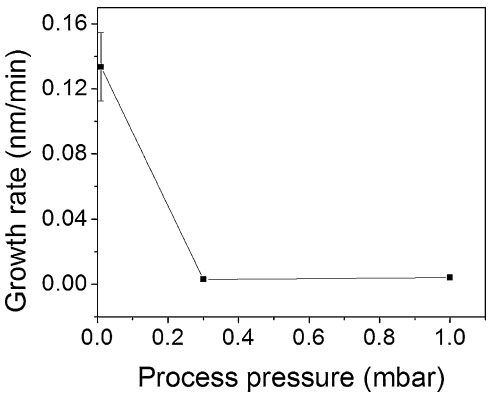

Figure 6 CVD growth rate versus process pressure during a 1 min exposure to at-H, after a 1-min exposure to WF_6 gas followed by a 2-min purge. Conditions: 325 °C of substrate temperature, 1750 °C of hot-wire temperature, 100 sccm of H_2, 2 sccm of WF_6, 100 sccm of H_2-carrier gas (Ar), and 50 sccm WF_6-carrier gas (Ar).

The influence of substrate temperature and total gas pressure on the net growth is shown in Fig. 8, which further illustrates the interplay between deposition and etching. It is obvious that etching is enhanced by a higher pressure resulting in a lower growth rate. Furthermore, etching becomes dominant at a lower temperature if the pressure is higher. Considering etching and deposition as two parallel reactions, an increase in substrate temperature results in a higher etching rate rather than a higher growth rate, we conclude that etching has a stronger dependence on substrate temperature compared to deposition. In order to achieve a higher growth rate, 315 °C was determined to be the substrate temperature for the following ALD experiments.

Pressure is clearly a crucial parameter in the interplay between deposition and etching. Furthermore, the net-deposition can be affected by both CVD and ALD, as both processes can contribute. For a CVD mode, lowering the total pressure is favorable as WF_6 can easier diffuse upwards to the hot hot-wire and decompose there. Therefore, at a

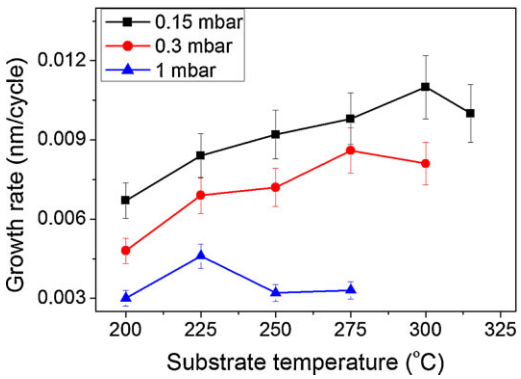

Figure 8 Influence of total pressure and substrate temperature on net growth. The cycle sequence: 10 s of H_2 (100 sccm)/30 s of Ar (purge)/0.1 s of WF_6 (2 sccm)/30 s of Ar (purge). Other conditions: Ar-carrier gas flow rate of 100 and 50 sccm for H_2 and WF_6, respectively; hot-wire temperature of 1750 °C. Due to the short pulse time of WF_6, its actual flow rate cannot be accurately measured.

higher pressure, lesser contribution from CVD may be expected. However, increasing the pressure will enhance simultaneous etching of the deposited film. Therefore, an optimum pressure must be found to achieve a balance (net-zero effect) between CVD and etching. In the corresponding experiment, WF_6 and at-H were mixed in gas phase to ensure CVD mode and no ALD, aiming to observe the interplay of CVD and etching. From Fig. 9, the maximum CVD growth is observed at the lowest pressure of 0.01 mbar, and growth rate decreases to 0.008 nm/min at 0.1 mbar. At 0.2 mbar, the net growth is already negative, meaning dominant etching. Therefore, pressure between 0.1 and 0.2 mbar was selected to provide a balance between CVD mode and etching.

3.3 Optimization of the HWALD process For an ideal ALD process, similar to CVD, the growth rate per

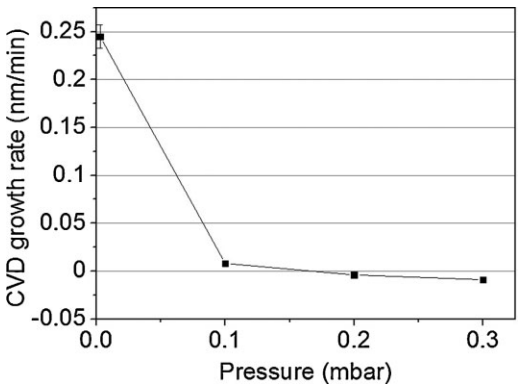

Figure 9 Influence of process pressure on the CVD growth rate when at-H and WF_6 were mixed. Conditions: 100 sccm of H_2, 2 sccm of WF_6, 100 sccm of H_2-carrier gas (Ar), and 50 sccm WF_6-carrier gas (Ar), hot-wire temperature of 1750 °C and substrate temperature of 315 °C.

cycle (GPC) can be very slow at the initial stage, due to nucleation. GPC is expected to settle to a constant value (i.e., reaching a linear-growth regime) when the surface has been fully covered by the ALD layer [31]. In this regime, GPC is expected to be independent of experimental parameters (a so-called ALD window) [1]. To determine the ALD window in our work, the at-H pulse time, hot-wire temperature, and the post at-H purge time were varied. The WF_6 pulse time and the total pressure were fixed at 0.1 s and 0.15 mbar, as discussed above, to provide optimal conditions for the HWALD. Figure 10 depicts the linear growth regime between 280 and 420 cycles. The inset shows the SE recorded points for a number of cycles. The time resolution of SE was 2.5 s, so the recorded points in every cycle were sufficient to delineate the growth. The one-cycle variations in the inset reflect the changes of optical properties of the surface upon exposure to different reactants. In other words, this would not necessarily be the actual thickness variations. However, the net thickness increases after each cycle should correspond to the actual films growth, as the final film thickness is verified by other techniques (HIM and XRR).

In Fig. 11(a–c) the GPC as a function of H_2 pulse time (a), filament temperature (b), and purge time (c) is shown. From these figures, an at-H pulse time of 10 s, a hot-wire temperature of 1750 °C, and a post at-H purge time of 20 s can be chosen to maintain an ALD mode. These parameters ensure a relatively-independent GPC. The at-H pulse time shorter than 10 s led to non-saturating surface reactions, where exposures longer than 20 s enhanced a CVD mode. The purge times shorter than 20 s also enhanced CVD and thereby increased GPC. Hot-wire temperatures exceeding 1750 °C negatively affected the ALD probably due to the

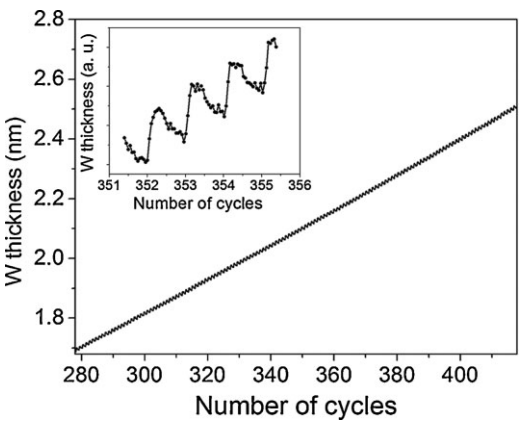

Figure 10 *In-situ* monitoring of HWALD growth in the linear regime by SE; the inset shows stepwise growth for individual cycles. Conditions: one ALD cycle consisted of 10 s H_2 (100 sccm)/20 s Ar (purge)/0.1 s WF_6 (2 sccm)/30 s Ar (purge). Other conditions: Ar-carrier gas flow rate of 100 sccm and 50 sccm for H_2 and WF_6, respectively; hot-wire temperature of 1750 °C; process pressure of 0.15 mbar and substrate temperature of 315 °C. Due to the short pulse time of WF_6, its actual flow rate cannot be accurately measured.

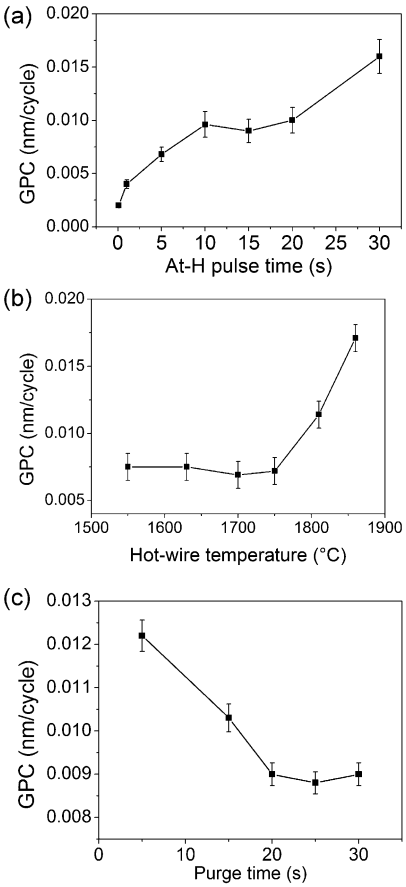

Figure 11 Determining HWALD windows. Influence of: (a) at-H pulse time, (b) hot-wire temperature, and (c) post at-H purge time. Standard parameter values: 0.15 mbar of pressure, 315 °C of substrate temperature, 1750 °C of hot-wire temperature, 100 sccm of H_2, 2 sccm of WF_6, 100 sccm of H_2-carrier gas (Ar), and 50 sccm WF_6-carrier gas (Ar). Each graph shows the influence of one parameter only while keeping the standard values for all other parameters. Due to the short pulse time of WF_6, its actual flow rate cannot be accurately measured.

enhancement of gas-phase reactions, again shifting the process towards CVD and increasing the GPC. The pulse time of WF_6 was limited at 0.1 s, to minimize the role of the permanent background reactants contributing to CVD and etching, as discussed in the previous sections. The post WF_6 purge time was fixed at 30 s; shorter times resulted again in net etching.

In Fig. 12, an XPS depth profile is shown of a 15 nm HWALD W film grown under the optimized conditions. As mentioned in Section 2.3, the top-5-nm film corresponds to the a-Si capping layer. The SE measurements reveal a thickness of 12.6 nm actual HWALD W layer on top of 2.3 nm W seed layer. The total thickness of 15 nm is in agreement with the estimate from the XPS sputter depth using the average sputter rates. Remarkably, the concentration of W approaches 99 at%.

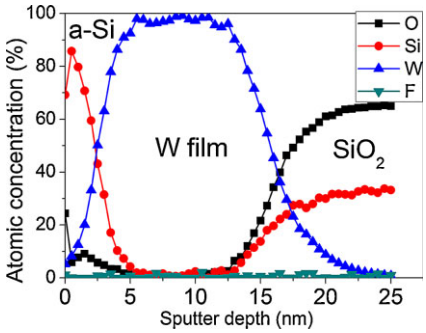

Figure 12 XPS depth profile of a 15-nm thick HWALD W film (shown in Fig. 10) resulted in high-purity W. One ALD cycle consisted of 10 s H_2 (100 sccm)/20 s Ar (purge)/0.1 s WF_6 (2 sccm)/30 s Ar (purge). Other conditions: Ar-carrier gas flow rate of 100 sccm and of 50 sccm for H_2 and WF_6, respectively; hot-wire temperature of 1750 °C; process pressure of 0.15 mbar and substrate temperature of 315 °C. Due to the short pulse time of WF_6, its actual flow rate cannot be accurately measured.

4 Summary and conclusion In this work, we studied a hot-wire assisted deposition of W films by sequential pulses of WF_6 and at-H precursors in a cold-wall reactor. We demonstrated the coexistence of CVD, etching, and ALD modes and investigated the influence of process parameters on each mode. This allowed to independently enhance a selected mode and supress the others. A higher gas pressure strengthened etching whereas a lower pressure could enhance CVD. By selecting proper process pressure, substrate and hot-wire temperature, precursor-pulse, and purge times, optimal conditions were found to maintain the ALD mode. Under these chosen conditions, HWALD W films were deposited with W purity approaching 99 at%.

Acknowledgment We thank the Dutch Technology foundation (STW) for the financial support of this project (STW-12846).

References

[1] S. M. George, Chem. Rev. **110**, 111 (2010).
[2] Y. J. Lee and S. W. Kang, Electrochem. Solid-State Lett. **5**, C91 (2002).
[3] Y. J. Lee and S. W. Kang, Thin Solid Films **446**, 227 (2004).
[4] C. Ozgit, I. Donmez, M. Alevli, and N. Biyikli, J. Vac. Sci. Technol. A **30**, 01A124–1 (2012).
[5] K. Devloo-Casier, D. Deduytsche, S. Van den Berghe, K. Driesen, and C. Detavernier, J. Solid State Sci. Technol. **1**, Q123 (2012).
[6] V. V. Afanas'ev, J. M. M. de Nijs, and P. Balk, J. Appl. Phys. **78**, 6481 (1995).
[7] A. H. Mahan, A. C. Dillon, L. M. Gedvilas, D. L. Williamson, and J. D. Perkins, J. Appl. Phys. **94**, 2360 (2003).
[8] A. H. Mahan, J. Carapella, B. P. Nelson, R. S. Crandall, and I. Balberg, J. Appl. Phys. **69**, 6728 (1991).
[9] I. Langmuir, J. Am. Chem. Soc. **34**, 860 (1912).
[10] I. Langmuir and G. M. J. Mackay, J. Am. Chem. Soc. **36**, 1708 (1914).

[11] I. Langmuir, J. Am. Chem. Soc. **37**, 417 (1915).
[12] H. Matsumura and H. Tachibana, Appl. Phys. Lett. **47**, 833 (1985).
[13] H. Shimizu, K. Sakoda, T. Momose, and Y. Shimogaki, Jpn. J. Appl. Phys. **51**, 05EB02 (2012).
[14] H. Shimizu, K. Sakoda, T. Momose, M. Koshi, and Y. Shimogaki, J. Vacuum Sci. Technol. A **30**, 01A144 (2012).
[15] I. Kostis, M. Vasilopoulou, G. Papadimitropoulos, N. Stathopoulos, S. Savaidis, and D. Davazoglou, Surf. Coat. Technol. **230**, 51 (2013).
[16] E. Lassner and W.-D. Schubert, Tungsten: Properties, Chemistry, Technology of the Element, Alloys, and Chemical Compounds (Kluwer Academic/Plenum Publishers, New York, 1999), p. 13.
[17] H. Van Bui, A. Y. Kovalgin, A. A. I. Aarnink, and R. A. M. Wolters, J. Solid State Sci. Technol. **2**, 149 (2013).
[18] J. N. Smith, Jr. and W. L. Fite, J. Chem. Phys. **37**, 898 (1962).
[19] J. E. J. Schmitz, Chemical Vapor Deposition of Tungsten and Tungsten Silicides for VLSI/ULSI Applications (Noyes Publications, Park Ridge, 1992), p. 12.
[20] T. Noma, K. Soo Seol, M. Fujimaki, and Y. Ohki, J. Appl. Phys. **85**, 8423 (1999).
[21] C. F. Klingshirn (ed.), Semiconductor Optics (Springer, Karlsruhe, 2012), p. 80.
[22] P. Patsalas and S. Logothetidis, J. Appl. Phys. **93**, 989 (2003).
[23] F. Wooten, Optical Properties of Solids (Academic Press, New York, 1972) p. 52.
[24] E. D. Palik (ed.), Handbook of Optical Constants of Solids (Academic Press, College Park, 1997), p. 577.
[25] C. M. Hezinger, B. D. Jonhs, W. A. McGahan, J. A. Woollam, and W. Paulson, J. Appl. Phys. **83**, 3323 (1998).
[26] G. Jellidon and F. Modine, Phys. Rev. B **27**, 7466 (1983).
[27] C-E Morosanu and V. Soltuz, Thin Solid Films **52**, 181 (1978).
[28] T. T. Kodas and M. J. Hampden-Smith (eds.), The Chemistry of Metal CVD (Wiley-VCH, Weinheim, 2008), p. 121.
[29] R. W. Boswell and R. K. Porteous, J. Appl. Phys. **62**, 3123 (1987).
[30] H. Wise and C. M. Ablow, J. Chem. Phys. **35**, 10 (1961).
[31] R. Puurunen, J. Appl. Phys. **97**, 121301 (2005).

